

Wear Independent Similarity

Adam Steele,[†] Alexander Davis,[†] Joohyung Kim,[†] Eric Loth,^{*,†} and Ilker S. Bayer[‡]

[†]Department of Mechanical and Aerospace Engineering University of Virginia 122 Engineer's Way P.O. Box 400746 Charlottesville, Virginia 22904, United States

[‡]Smart Materials, Nanophysics, Istituto Italiano di Tecnologia Via Morego, 30, 16163 Genova, Italy

ABSTRACT: This study presents a new factor that can be used to design materials where desired surface properties must be retained under in-system wear and abrasion. To demonstrate this factor, a synthetic nonwetting coating is presented that retains chemical and geometric performance as material is removed under multiple wear conditions: a coarse vitrified abrasant (similar to sanding), a smooth abrasant (similar to rubbing), and a mild abrasant (a blend of sanding and rubbing). With this approach, such a nonwetting material displays unprecedented mechanical durability while maintaining desired performance under a range of demanding conditions. This performance, herein termed wear independent similarity performance (WISP), is critical because multiple mechanisms and/or modes of wear can be expected to occur in many typical applications, e.g., combinations of abrasion, rubbing, contact fatigue, weathering, particle impact, etc. Furthermore, these multiple wear mechanisms tend to quickly degrade a novel surface's unique performance, and thus many promising surfaces and materials never scale out of research laboratories. Dynamic goniometry and scanning electron microscopy results presented herein provide insight into these underlying mechanisms, which may also be applied to other coatings and materials.

KEYWORDS: nanocomposite, wear, wettability, superhydrophobic, coating, abrasion

Wear independent similarity of a nonwetting nanocomposite



INTRODUCTION

Approaches to enhance interface performance from novel combinations of physical and chemical effects have stimulated the fabrication of a range of surfaces and materials with robust micro- and nanostructured morphologies. Specifically, remarkable properties in wetting, adhesion, thermal and/or electrical conductivity,¹ optical activity, and capability to direct cell growth have all been shown to result from textured surfaces.² Such properties are of interest for a wide variety of applications including energy storage and conversion, medical devices, microelectronics, and chemical and biological sensing. However, fabrication of such surface features often pushes the limits of their mechanical durability, making it challenging to produce the desired surfaces in a scalable and cost-effective manner. Furthermore, the multiple wear modes that exist in typical applications tend to quickly degrade a novel surface's unique performance, and thus many promising surfaces and materials never scale out of research laboratories. One field where this trade-off has been especially limiting is in nonwetting surfaces.

Nonwetting materials originate in nature including plant leaves, duck feathers, and insects.³ Their characteristic micro and nano surface morphology combined with low surface energy chemical functionality were first synthetically created by Wenzel⁴ in the late 1930s and then by Cassie and Baxter⁵ in the early 1940s.⁶ In the last 25 years, more than a thousand studies have been published and a wide array of approaches have been developed for creating nonwetting surfaces.⁷ These materials have potential in many applications such as drag reduction for

marine vehicles and fluid power systems, antifouling on aircraft and wind turbines, and stain-resistant coatings.

Most studies define superhydrophobic performance based on water contact angles (CA) of at least 150° as well as contact angle hysteresis (CAH) and roll-off angle (ROA) values less than 10–20°. High antiwettability to other liquids such as oils⁸ and alkanes⁹ have even been reported. In the past few years, several studies have reported relatively simple and economical fabrication techniques applicable to large surface area application,^{10–12} some with environmentally friendly compositions.¹³ However, a critical remaining hurdle that must be overcome for industrial application is suitable mechanical durability, because most nonwetting coatings are extremely fragile. Investigation into the mechanical durability of nonwetting surfaces has therefore become of recent interest.¹⁴ Superhydrophobic functionalized textiles have shown significant durability potential.¹⁵ Unfortunately, the same technique applied to solid substrates showed almost no durability under the same conditions. While several studies claim durable superhydrophobic surfaces on solid flat substrates, generally this durability is based on relatively mild tests such as low pressure water flow,^{16,17} outdoor exposure,¹⁸ and milli-Newton scale tribometer tests.¹⁹

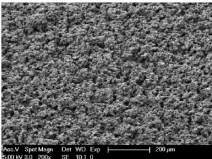
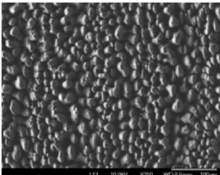
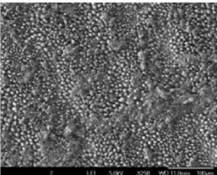
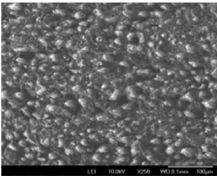
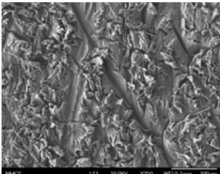
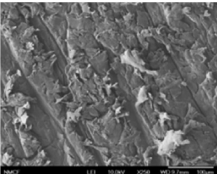
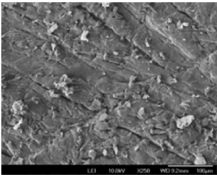
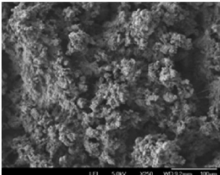
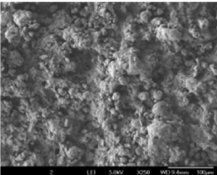
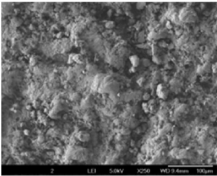
In general, there are two approaches to creating a durable nonwetting surface: (1) limiting material removal so as to retain

Received: January 23, 2015

Accepted: May 27, 2015

Published: May 27, 2015

Table 1. Summary of Mechanical Durability Results As Tested in Lab with H18 Vitrified Abradant for Five (Initially) Superhydrophobic Surfaces in Order of Increasing Wear Resistance (250X Magnification)

Surface	As Is	Droplet Pinned After X Abrasion Cycles	After 15 Abrasion Cycles
Fluoropolymer / ZnO Nanocomposite Coating ⁸	 CA = 162° CAH = 4°	Surface destroyed after 1 cycle	Surface destroyed after 1 cycle
Laser-Textured Titanium ²⁰	 CA = 160° CAH = 8°	 CA = 117° CAH = pinned 2 cycles	 CA = 93° CAH = pinned
Sanded Teflon ¹¹	 CA = 149° CAH = 13°	 CA = 126° CAH = pinned 3 cycles	 CA = 76° CAH = pinned
PUR / Fluoropolymer / Nanoclay Nanocomposite Coating ²⁹	 CA = 156° CAH = 7°	 CA = 121° CAH = pinned 5 cycles	 CA = 106° CAH = pinned

superhydrophobicity under wear for as long as possible^{20–23} and (2) developing a material that maintains superhydrophobicity as it wears away.^{11,24–27} For the latter type, such performance for surfaces under a *single* wear condition is herein defined as “wear similarity”. A simple example of wear similarity is sanded Teflon which can be rendered superhydrophobic by using a fine grit sandpaper¹¹ so that continued sanding would retain superhydrophobicity until the Teflon material is completely worn away. There are other examples of wear similarity with respect to manual sanding, but these do not demonstrate wear similarity over a wide range of abrasion conditions typical of most applications. For example, the superhydrophobic sanded Teflon surface would lose its performance if subjected to a different type of wear (as will be shown herein).

In the current work, we present an approach for designing nanocomposite coatings that demonstrate wear independent similarity performance (WISP), herein defined as maintaining surface performance as material is removed under *multiple* wear conditions. The concept of wear independent similarity is inspired by natural surfaces such as tooth enamel, which can

retain specialized surface characteristics under mechanical wear. For instance, nanoscale roughness and porosity combined with surface chemistry can be maintained under a range of wear conditions allowing for diffusion of calcium and phosphate into the tooth surface while preventing bacterial adherence.²⁸

■ EXPERIMENTAL METHODS

Four nonwetting surfaces were first fabricated to characterize their performance under linear abrasion to provide perspective. These surfaces are based on previous studies and include laser-textured titanium,²⁰ sanded Teflon,¹¹ a fluoropolymer:ZnO nanocomposite,⁸ and a polyurethane(PUR):fluoropolymer:nanoclay nanocomposite.²⁹ In addition, a fifth nanocomposite coating was developed to specifically have wear independent similarity performance. This WISP-designed coating was applied to a 3 × 3 in. square substrate of 6061 aluminum alloy (McMasterr-Carr), initially cleaned with isopropyl alcohol. The aluminum surface was then sprayed with a commercial general purpose spray adhesive (3 M 45) from a distance of about 10 cm, creating a continuous layer of adhesive. Next, a dispersion of 25 nm Aerosil R812 hydrophobic fumed silica in acetone (with a concentration of 0.025 g/mL) was then sprayed from a distance of about 30 cm using an HLVP spray gun (SATA Minijet

3000B) while the adhesive layer was still tacky. The resulting surface was immediately superhydrophobic owing to the rough structure of the hydrophobic silica created through spraying but was air-dried at room temperature for 24 h before abrasion testing. To provide different types of wear conditions and quantitatively investigate nonwetting durability, a linear abraser was used in combination with measurements of water contact angle and hysteresis as discussed below.

The linear abraser (Taber Linear Abraser, Taber Industries, USA) employed three different abrasants: the H-18 vitrified abrasant (similar to coarse sanding), crocking cloth abrasant (similar to rubbing), and CS-10F mild abrasant (a blend of mild sanding and rubbing). The normal load during abrasion was fixed for this study at 416 g with a fixed cycle velocity of 3 cm/s. Given the contact area of the abrasant (based on 0.25 in. radius abrasants), these conditions correspond to a mechanical pressure of 32.2 kPa. The morphological analysis of the samples before and after abrasion testing were carried out using an SEM (JEOL 6700F and FEI Quanta 650). To characterize the baseline effect of abrasion on wetting properties, a bare piece of 6061 aluminum alloy was abraded and evaluated with energy-dispersive X-ray spectroscopy (EDXS) (JEOL-6700F with PGT IMIX-SPIRIT EDXS detector). Although contact angle increased slightly during abrasion due to roughening the baseline aluminum surface, EDXS showed no discernible chemical change to the surface. This test indicates that surface changes due to the linear abraser are primarily morphological.

A goniometer (ramé-hart model 290) was used to capture static and dynamic 10 μL water droplet images on a custom tilt stage designed for the linear abraser. The droplet was produced at the tip of a syringe at approximately 1 $\mu\text{L}/\text{s}$ dispense flow rate. The syringe tip was sized such that the droplet released from the tip before 10 μL . Thus, before 10 μL was reached, the droplet was slowly lowered onto the surface, at which point the remaining volume was dispensed before slowly retracting the syringe tip. The stage could be tilted, and upon droplet rolling or sliding, dynamic contact angle measurement could be performed. This process ensured that no kinetic effects in which the contact angle changes on a time scale that is comparable to the time of the measurement were observed. Thus, thermodynamic hysteresis was the primary effect associated with the measured differences between advancing and receding contact angles. ImageJ software was used to process the images with a Java plugin (Drop Shape Analysis, Stalder)³⁰ to calculate the static and dynamic contact angles. Each contact angle or roll-off angle data point in this study represents an average of three measurement locations on the sample. Estimated uncertainty for this method is $\pm 5^\circ$ for contact angles and $\pm 3^\circ$ for roll-off angles.

RESULTS AND DISCUSSION

The nonwetting performance results under linear abrasion for the first four surfaces are reported in Table 1. These results provide a quantitative basis for the present setup and illustrate the difficulty in creating mechanically durable nonwetting surfaces. For example, the first coating, a nanocomposite composed of a fluoropolymer binder with clay nanoparticle filler, was destroyed completely after just one cycle. This low mechanical durability results from the lack of a strong binder, which is typical for many superhydrophobicity studies in the literature.

The second coating in this table shows that a laser-textured titanium surface loses its superhydrophobic performance after just two abrasion cycles, indicating even the strongest materials (titanium is highly mechanically durable) can have their microstructure worn relatively quickly in this abrasion system. The third surface in Table 1 is a superhydrophobic surface created by sanding a Teflon plate.¹¹ Even though its microtexture was created by sanding, it lost its superhydrophobic performance after three abrasion cycles with this abrasant. This result illustrates that highly specialized

conditions are needed to create and maintain a superhydrophobic surface on Teflon via sanding (a certain grit size sanded in a circular motion). In other words, superhydrophobic Teflon via sanding demonstrates wear similarity that is wear dependent. It is wear similar under a certain grit size sanded in a circular motion, but it is not wear similar under other wear conditions such as H18 vitrified linear abrasion as demonstrated in Table 1. Note that linear abrasion with the crocking cloth abrasant and CS-10F mild abrasant on the superhydrophobic Teflon surface yielded similar results to the H18 vitrified abrasant for this case. Similarly, nanocomposite materials have shown wear similarity that is wear dependent to specialized sanding,²⁴ whereby superhydrophobic wear similarity is only achieved if the act of sanding imparts a surface structure similar to that initially created, e.g., micrometer scale asperities spaced tens of micrometers apart, but other wear conditions also quickly degraded its nonwetting properties. The fourth surface in Table 1 is a nanocomposite with a binder composed of an interpenetrating polymer network of polyurethane and a fluoropolymer with a clay nanoparticle filler. Although such a coating demonstrated very high substrate adhesion,²⁹ superhydrophobicity was lost after just five abrasion cycles. Thus, the results of Table 1 demonstrate that this abrasion system, which is generally accepted as a standard method for wear testing, does not inherently allow wear similarity in contrast to the sanding-type mechanisms popularly applied in the literature.^{11,24–27}

The WISP nanocomposite (Figure 1) created in this study was first tested for wear similarity under linear abrasion using

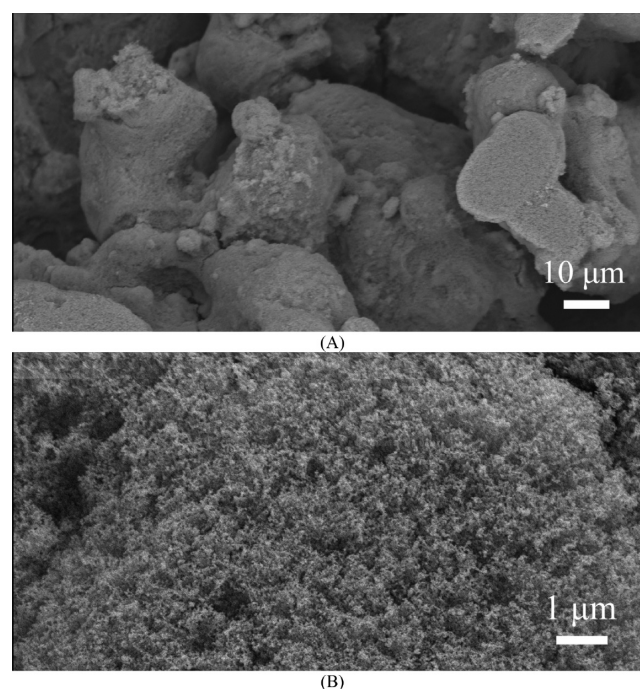


Figure 1. Representative SEM images of the fifth surface (WISP nanocomposite) showing both micro- and nanoscale surface structure based on magnifications of (A) 600 \times and (B) 8000 \times .

the H-18 vitrified abrasant for coarse abrasive wear. These results are shown in Figure 2 and compared against laser-textured titanium and the PUR:fluoropolymer:nano-clay nanocomposite. It can be observed in Figure 2A–C that the advancing CA, CAH, and ROA curves for the WISP

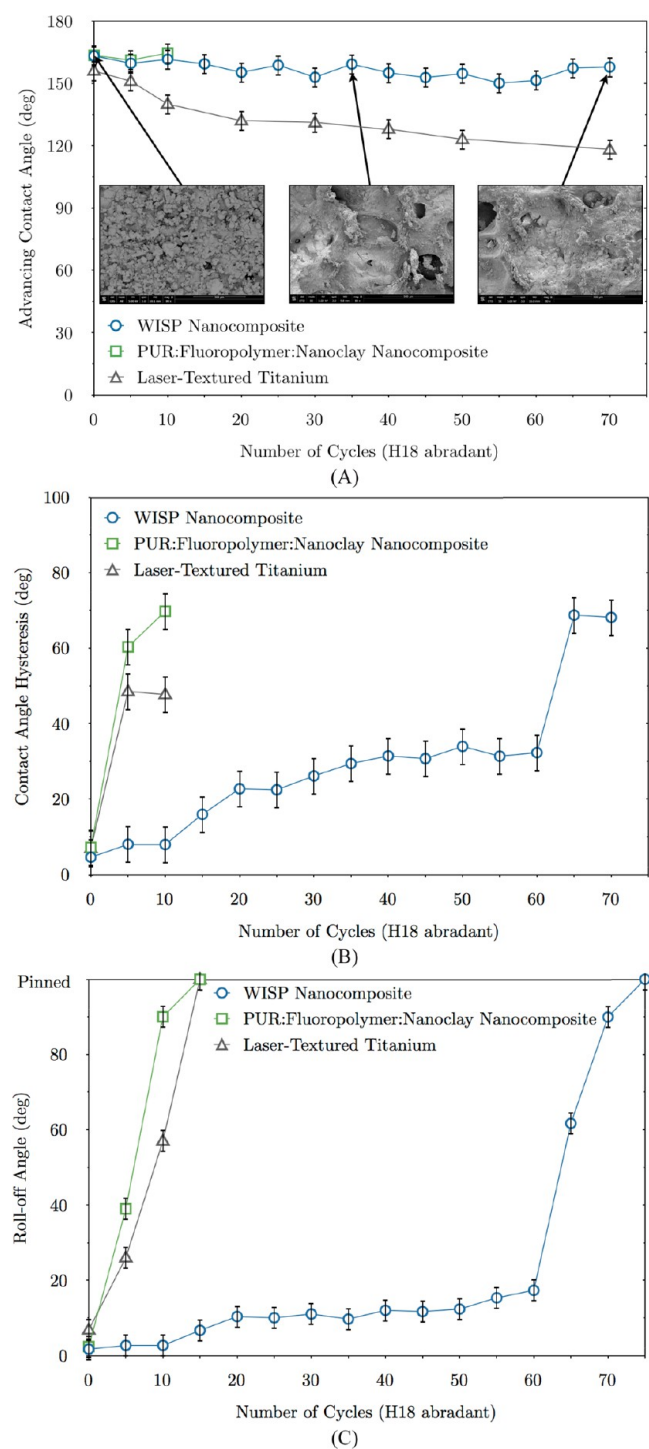


Figure 2. (A) CA, (B) CAH, and (C) ROA vs number of linear abrasion cycles using H18 abrasant showing wear similarity of WISP nanocomposite (with SEM inset images at 80 \times magnification) compared to other superhydrophobic surfaces.

nanocomposite retained high nonwetting performance for 60–70 abrasion cycles. This is in stark contrast to the other surfaces where superhydrophobic performance was lost after just one cycle. Although the PUR:fluoropolymer:nanoclay nanocomposite had a relatively constant advancing CA for 10 abrasion cycles, the CAH and ROA increased quickly and at 15 cycles the coating suddenly failed, revealing the underlying substrate. A different degradation behavior was observed for the laser-

textured titanium surface as it did not fail; rather, the advancing CA gradually decreased with an increasing number of cycles whereas the CAH and ROA increased rapidly and droplets pinned at 15 cycles. Interestingly, for the WISP surface, the CAH and ROA degraded first, while the advancing CA remained high even after coating breakthrough due to residual microfeatures on the aluminum substrate. An important conclusion from Figure 2 is that the WISP nanocomposite was the only surface that demonstrated wear similarity under this condition. In particular, it retained superhydrophobic or near-superhydrophobic performance during abrasion up to the point of coating removal, when the underlying substrate was revealed at cycle 65 (Figure 2B,C). The other four surfaces did not demonstrate wear similarity under this condition (as shown in Table 1 and Figure 2) even though they may show wear similarity under other conditions, e.g., the Teflon sanded surface retains its superhydrophobic performance if instead subjected to certain fine grit sanding and is thus shows wear similarity that is wear-dependent.

The WISP nanocomposite was then tested to determine whether its design actually yielded wear independent similarity, i.e., maintaining surface performance while subject to wear under different conditions. The results are shown in Figure 3 for three wear conditions: coarse wear, mild wear, and rubbing wear. It can be observed that the advancing CA, CAH, and ROA curves collapse onto each other and remain relatively flat over multiple wear conditions. This is the first report of wear independent similarity for a nonwetting material. It can also be observed that each wear condition had a different wear rate, causing the underlying substrate to be revealed at a different point for each abrasant (Figure 3B,C). Once the underlying hydrophilic aluminum substrate was revealed, the nonwetting performance began to degrade as more and more substrate area was exposed after each additional abrasion cycle.

Analysis of the SEM images provides insight into these results. Figure 4 shows SEM images of the WISP nanocomposite at 80 \times magnification after 35 linear abrasion cycles for each wear condition (note abrasion direction). It is apparent from comparing the images that the surface structure is similar in two distinct ways. First, there is an appearance of relatively large diameter cavities which indicates material has been peeled away throughout the surface. This is confirmed with the appearance of rolled-up residual material at the trailing edge of these cavities, i.e., in the direction of the last abrasion cycle. Second, arrays of much smaller surface asperities approximately 1–10 μm in scale can be observed interspersed between the larger peeling. It is also noted that the microstructure size of the WISP nanocomposite varies from 10 to 100 μm , which is most similar to the microstructure size of the H18 abrasant (average particle size approximately 100 μm). Thus, the least amount of 10 μm scale residual material and wear is produced with the H18 abrasant as observed in Figure 4A, compared to the smaller microstructure of the CS-10F (average particle size approximately 40 μm) and crocking cloth (average fiber diameter approximately 20 μm) which produces more 10 μm scale residual material as observed in Figure 4B,C. The larger load per particle of the H18 abrasant also causes more cavities and with a larger average diameter as observed in Figure 4A compared to Figure 4B,C.

Upon closer inspection of these smaller surface asperities as shown in Figure 5A, it is observed that linear abrasion caused structural failure via fracturing under each wear condition. As seen in Figure 1 and the inset in Figure 2A, these cavities,

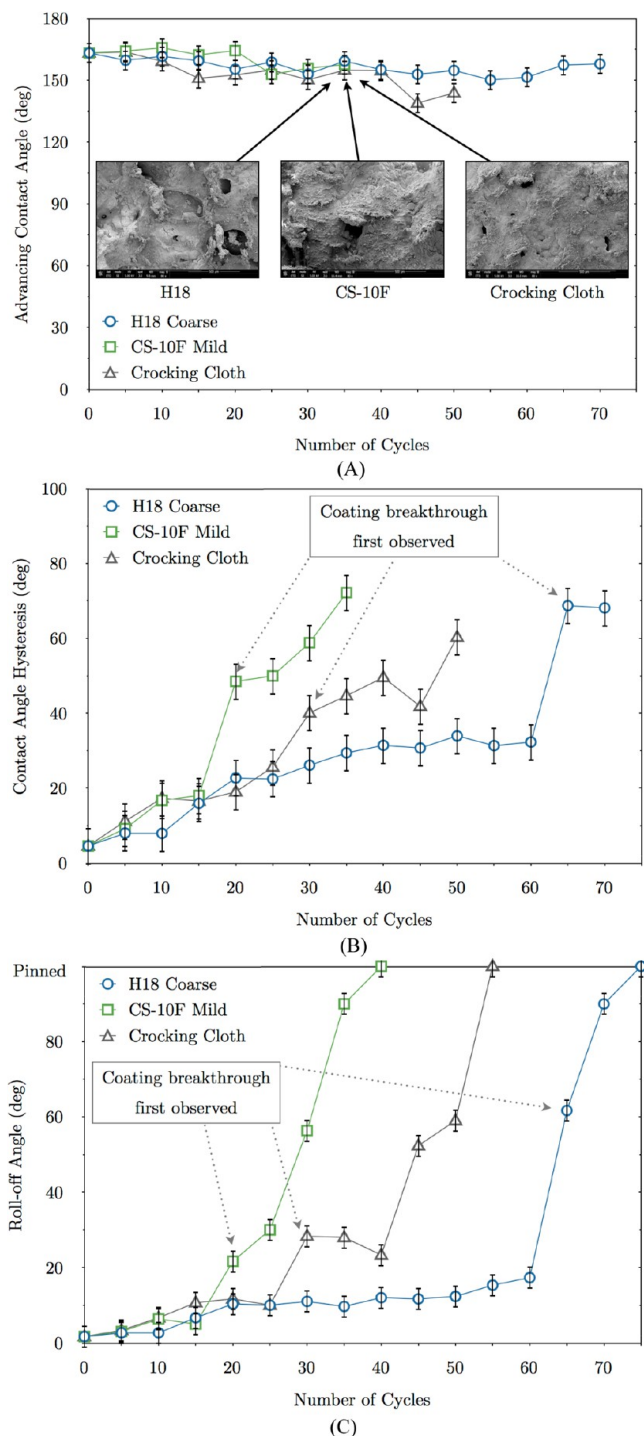


Figure 3. (A) CA, (B) CAH, and (C) ROA vs number of linear abrasion cycles for various surfaces showing wear independent similarity of WISP nanocomposite up to point of coating breakthrough (with SEM inset images at 80 \times magnification).

residual material, and fracturing were not present before abrasion. This indicates that the WISP nanocomposite surface does not smooth, in contrast to the smoothing that occurs on most nonwetting surfaces depending on the wear conditions, e.g., compare the WISP nanocomposite of Figure 5A with a superhydrophobic nanocomposite from the literature of Figure 5B. Smoothing tends to plastically deform the surface morphology and destroy the required roughness for a

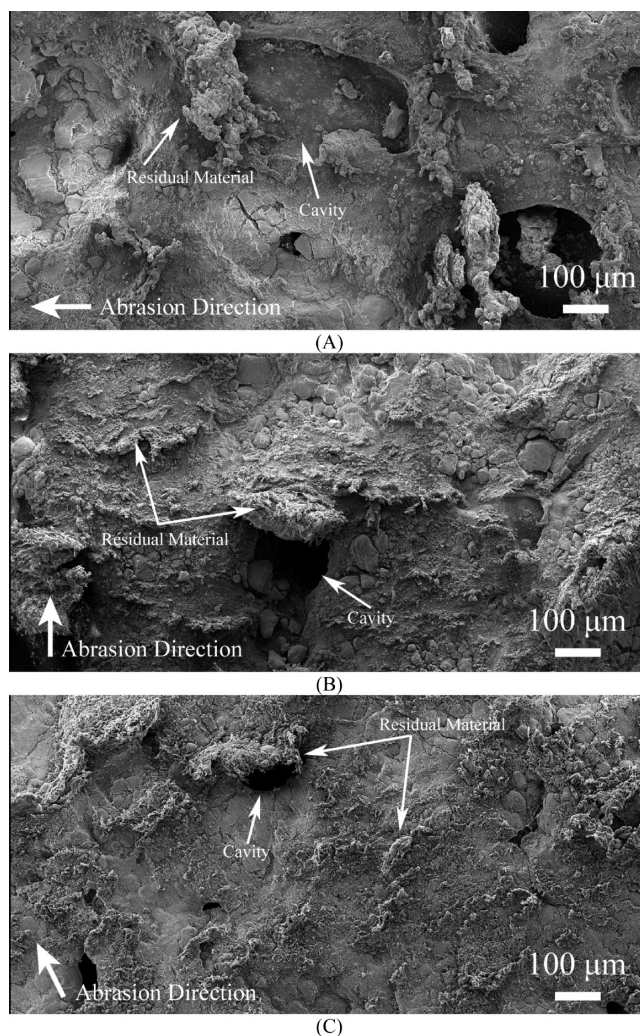


Figure 4. SEM images of WISP nanocomposite at 80 \times magnification after 35 linear abrasion cycles using (A) H18 vitrified harsh abrasant, (B) CS-10F resilient abrasant, and (C) crocking cloth abrasant. Note the abrasion direction in the bottom left of the images.

nonwetting surface. Thus, for wear independent similarity, the surface must be able to resist smoothing.

The WISP nanocomposite is able to resist smoothing under multiple conditions by fracturing before plastic deformation can dominate. This capability is accomplished in part by using a nanoparticle filler with increased hardness to resist nanoscale smoothing. The silica used in the WISP nanocomposite has a Mohs hardness of 7, compared to other typical particles such as zinc oxide (Mohs 4.5), titanium dioxide (Mohs 5.5), montmorillonite nanoclay (Mohs 2), and polytetrafluoroethylene (PTFE). However, the adhesive binder used in the WISP coating remains relatively soft and sticky upon curing, similar to the adhesive layer found on common sticky tapes. Upon spraying silica nanoparticles as a second step before the adhesive layer cures, the particles tend to agglomerate in shell-like clusters around the adhesive matrix. Thus, the outer layer of particles maintain a hard shell during wear, so when the mechanical forces become too great, rather than plastically deforming and smoothing, the nanoparticle layer fractures. When the underlying sticky adhesive binder is exposed, it tends to chemically adhere to the wearing surface, thereby allowing adhesive wear to dominate rather than other wear mechanisms

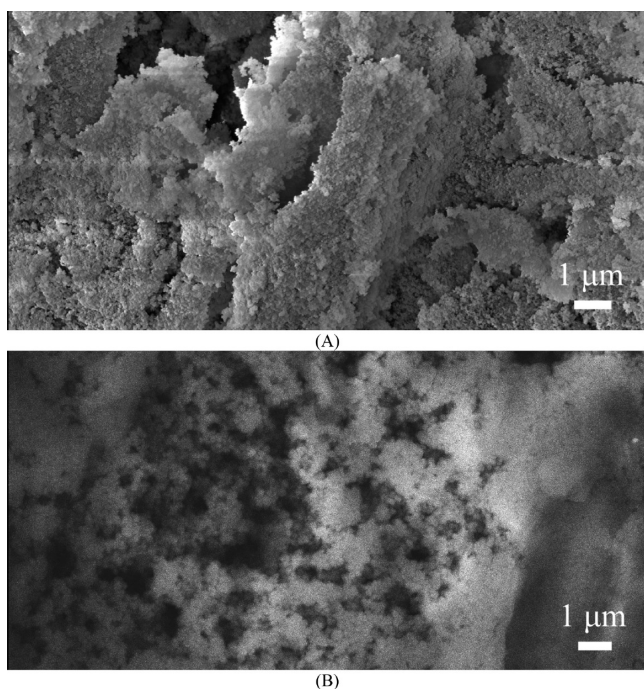


Figure 5. SEM images of surface features after linear abrasion with crocking cloth abrasant which demonstrates differences between (A) a WISP nanocomposite at 6000 \times magnification showing how surface fracture preserves micro- and nanostructure and (B) a non-WISP nanocomposite at 5000 \times magnification showing loss of surface texture as micro- and nanostructure is smoothed.

such as abrasion or contact fatigue. In other words, wear mechanism transition occurs, from abrasion to adhesive wear. During adhesive wear, contact and bonding take place at the interface, and these contacts are sheared during sliding, which results in residual material and detachment of surface fragments.³¹ This residual material tends to build up as sliding continues, creating new asperities at various scales depending on the amount of adhesion. These new asperities of residual material thus maintain the necessary rough surface morphology required for superhydrophobicity. This behavior and resulting morphology is clearly observed in Figure 4, where peeling and residual material buildup can be seen at various stages and scales.

To establish that the behavior observed is not simply a case of wear mode transition, a wear mode transition model from the literature is used to identify the dominant mode between two-body abrasion (grooving abrasion) and three-body abrasion (rolling abrasion).^{32,33} The critical condition for the transition from two-body to three-body abrasion is a function of the severity of contact and the hardness ratio between the surface and the abrasant. The relevant parameters are estimated as follows: the applied mechanical pressure is 32.2 kPa, the silica nanoparticle hardness is estimated between 2.8 and 9.65 GPa,^{34,35} the aluminum oxide abrasive particle hardness of the H18 and CS-10F abrasants are estimated between 13 and 29 GPa,³⁶ and the volume fraction of abrasive particles is estimated between 0.5 and 1. Thus, the severity of contact is on the order of 10^{-5} for all values and the hardness ratio is 0.1 to 0.7. When compared to the wear mode map in the model, in all cases with either the H18 or CS-10F abrasant, the abrasion falls well within the three-body region. This result is also supported by the fact that no grooves are observed in any of the SEM images

when using these abrasants on the WISP nanocomposite (unlike the sanded Teflon as observed in Table 1). On the other hand, for crocking cloth, the volume fraction of abrasive particles effectively approaches zero and thus linear abrasion with the crocking cloth falls well within the two-body region. Therefore, in all cases in the current study, the abrasion does not occur near the critical condition for wear mode transition, supporting the previous analysis that wear mechanism transition from abrasion to adhesive wear is producing the observed wear independent similarity.

As may be expected, the present results indicate that it is easiest for a WISP coating to resist smoothing under a coarse abrasant, as shown in Figure 3. The reason for this is that a coarse abrasant ensures the smallest surface area for adhesive contact so that less material may be removed. In addition, the coarse abrasant mainly produced larger cavities and residual material via adhesive wear as shown in Figure 4A. Under mild wear and rubbing wear, the WISP nanocomposite also resists smoothing, but finer abrasants tend to adhere to a larger percentage of the adhesive binder due to a larger average contact area. Thus, the milder and smoother abrasants simultaneously peel both large and small sections of the coating (Figure 4B,C) and more quickly reveal the underlying substrate. However, it is important to note that the rate of material removal for the WISP nanocomposite, regardless of the abrasant, was small compared to all other surfaces tested. This indicates that this surface has both high mechanical durability (low material removal) as well as wear independent similarity (retention of nonwetting performance as surface is removed under different wear conditions).

CONCLUSION

The present study shows a new factor that can be used to design materials where desired surface properties must be retained under in-system wear and abrasion. To demonstrate this factor, a synthetic nonwetting coating is presented that retains chemical and geometric morphology as material is removed under multiple wear conditions throughout the thickness of the material, i.e., wear independent similarity performance (WISP). This characteristic is critical for many practical applications that require lasting surface performance because multiple mechanisms and modes of wear can be expected. Dynamic goniometry and scanning electron microscopy revealed that for wear independent similarity in nonwetting materials, the surface must be able to resist smoothing to meet this requirement. The WISP nanocomposite accomplishes this under multiple conditions using a combination of hard nanoparticles which form shells that are integrated into an adhesive binder to promote adhesive fracturing and adhesive wear before smoothing can dominate.

AUTHOR INFORMATION

Corresponding Author

*E-mail: loth@virginia.edu.

Notes

The authors declare no competing financial interest.

ACKNOWLEDGMENTS

We acknowledge Yong Yeong and Athanasios Milonis for their assistance in the experiments and the support of the University of Minnesota and the National Science Foundation under grant no. NSF/EFRI-1038294.

■ REFERENCES

- (1) Wang, K.-X.; Li, X.-H.; Chen, J.-S. Surface and Interface Engineering of Electrode Materials for Lithium-Ion Batteries. *Adv. Mater.* **2015**, *27* (3), 527–545.
- (2) Tawfik, S.; De Volder, M.; Copic, D.; Park, S. J.; Oliver, C. R.; Polsen, E. S.; Roberts, M. J.; Hart, A. J. Engineering of Micro- and Nanostructured Surfaces with Anisotropic Geometries and Properties. *Adv. Mater.* **2012**, *24* (13), 1628–1674.
- (3) Bocquet, L.; Lauga, E.; Smooth, A. Future? *Nature Mater.* **2011**, *10* (5), 334–337.
- (4) Wenzel, R. N. Resistance of Solid Surfaces to Wetting by Water. *Ind. Eng. Chem.* **1936**, *28* (8), 988–994.
- (5) Cassie, A. B. D.; Baxter, S. Wettability of Porous Surfaces. *Trans. Faraday Soc.* **1944**, *40*, 546–551.
- (6) Lafuma, A.; Quere, D. Superhydrophobic States. *Nature Mater.* **2003**, *2* (7), 457–460.
- (7) Feng, X. J.; Jiang, L. Design and Creation of Superwetting/Antiwetting Surfaces. *Adv. Mater.* **2006**, *18* (23), 3063–3078.
- (8) Steele, A.; Bayer, I.; Loth, E. Inherently Superoleophobic Nanocomposite Coatings by Spray Atomization. *Nano Lett.* **2008**, *9* (1), 501–505.
- (9) Kota, A. K.; Li, Y.; Mabry, J. M.; Tuteja, A. Hierarchically Structured Superoleophobic Surfaces with Ultralow Contact Angle Hysteresis. *Adv. Mater.* **2012**, *24* (43), 5838–5843.
- (10) Bayer, I. S.; Steele, A.; Martorana, P. J.; Loth, E. Fabrication of Superhydrophobic Polyurethane/Organoclay Nano-structured Composites from Cyclomethicone-in-Water Emulsions. *Appl. Surf. Sci.* **2010**, *257* (3), 823–826.
- (11) Nilsson, M. A.; Daniello, R. J.; Rothstein, J. P.; Novel, A. and Inexpensive Technique for Creating Superhydrophobic Surfaces using Teflon and Sandpaper. *J. Phys. D: Appl. Phys.* **2010**, *43* (4), 045301.
- (12) Erbil, H. Y.; Demirel, A. L.; A, Y.; Mert, O. Transformation of a Simple Plastic into a Superhydrophobic Surface. *Science* **2003**, *299* (5611), 1377–1380.
- (13) Bayer, I. S.; Steele, A.; Martorana, P.; Loth, E.; Robinson, S. J.; Stevenson, D. Biolubricant Induced Phase Inversion and Superhydrophobicity in Rubber-Toughened Biopolymer/Organoclay Nanocomposites. *Appl. Phys. Lett.* **2009**, *95* (6), 063702-3.
- (14) Verho, T.; Bower, C.; Andrew, P.; Franssila, S.; Ikkala, O.; Ras, R. H. A. Mechanically Durable Superhydrophobic Surfaces. *Adv. Mater.* **2011**, *23* (5), 673–678.
- (15) Zimmermann, J.; Reifler, F. A.; Fortunato, G.; Gerhardt, L.-C.; Seeger, S. A Simple, One-Step Approach to Durable and Robust Superhydrophobic Textiles. *Adv. Funct. Mater.* **2008**, *18* (22), 3662–3669.
- (16) Cui, Z.; Yin, L.; Wang, Q.; Ding, J.; Chen, Q. A Facile Dip-Coating Process for Preparing Highly Durable Superhydrophobic Surface with Multi-scale Structures on Paint Films. *J. Colloid Interface Sci.* **2009**, *337* (2), 531–537.
- (17) Cui, Z.; Wang, Q.; Xiao, Y.; Su, C.; Chen, Q. The Stability of Superhydrophobic Surfaces Tested by High Speed Current Scouring. *Appl. Surf. Sci.* **2008**, *254* (10), 2911–2916.
- (18) Manca, M.; Cannavale, A.; De Marco, L.; Aricò, A. S.; Cingolani, R.; Gigli, G. Durable Superhydrophobic and Antireflective Surfaces by Trimethylsilanized Silica Nanoparticles-Based Sol–Gel Processing. *Langmuir* **2009**, *25* (11), 6357–6362.
- (19) Jung, Y. C.; Bhushan, B. Mechanically Durable Carbon Nanotube Composite Hierarchical Structures with Superhydrophobicity, Self-Cleaning, and Low-Drag. *ACS Nano* **2009**, *3* (12), 4155–4163.
- (20) Steele, A.; Nayak, B. K.; Davis, A.; Gupta, M. C.; Loth, E. Linear Abrasion of a Titanium Superhydrophobic Surface Prepared by Ultrafast Laser Microtexturing. *J. Microeng. Microtech.* **2013**, *23* (11), 115012.
- (21) Huovinen, E.; Hirvi, J.; Suvanto, M.; Pakkanen, T. A. Micro–Micro Hierarchy Replacing Micro–Nano Hierarchy: A Precisely Controlled Way To Produce Wear-Resistant Superhydrophobic Polymer Surfaces. *Langmuir* **2012**, *28* (41), 14747–14755.
- (22) Yonghao, X.; Yan, L.; Balu, B.; Hess, D. W.; Chingping, W. Robust Superhydrophobic Surfaces Prepared With Epoxy Resin and Silica Nanoparticles. *IEEE Trans. Compon., Packag., Manuf. Technol.* **2012**, *2* (3), 395–401.
- (23) Xu, Q. F.; Mondal, B.; Lyons, A. M. Fabricating Superhydrophobic Polymer Surfaces with Excellent Abrasion Resistance by a Simple Lamination Templating Method. *ACS Appl. Mater. Interfaces* **2011**, *3* (9), 3508–3514.
- (24) Bayer, I. S.; Brown, A.; Steele, A.; Loth, E. Transforming Anaerobic Adhesives into Highly Durable and Abrasion Resistant Superhydrophobic Organoclay Nanocomposite Films: A New Hybrid Spray Adhesive for Tough Superhydrophobicity. *Appl. Phys. Express* **2009**, *2* (125003), 125003.
- (25) Larmour, I. A.; Saunders, G. C.; Bell, S. E. J. Compressed Metal Powders that Remain Superhydrophobic after Abrasion. *ACS Appl. Mater. Interfaces* **2010**, *2* (10), 2703–2706.
- (26) Jin, H.; Tian, X.; Ikkala, O.; Ras, R. H. A. Preservation of Superhydrophobic and Superoleophobic Properties upon Wear Damage. *ACS Appl. Mater. Interfaces* **2013**, *5* (3), 485–488.
- (27) Zhu, X.; Zhang, Z.; Yang, J.; Xu, X.; Men, X.; Zhou, X. Facile Fabrication of a Superhydrophobic Fabric with Mechanical Stability and Easy-Repairability. *J. Colloid Interface Sci.* **2012**, *380* (1), 182–186.
- (28) Selwitz, R. H.; Ismail, A. I.; Pitts, N. B. Dental Caries. *Lancet* **2007**, *369* (9555), 51–59.
- (29) Steele, A.; Bayer, I.; Loth, E. Adhesion Strength and Superhydrophobicity of Polyurethane/Organoclay Nanocomposite Coatings. *J. Appl. Polym. Sci.* **2012**, *125* (S1), E445–E452.
- (30) Stalder, A. F.; Kulik, G.; Sage, D.; Barbieri, L.; Hoffmann, P. A Snake-Based Approach to Accurate Determination of Both Contact Points and Contact Angles. *Colloids Surf., A* **2006**, *286* (1–3), 92–103.
- (31) Sahoo, P. *Engineering Tribology*; Prentice-Hall of India Pvt.Ltd: New Delhi, 2005.
- (32) Adachi, K.; Hutchings, I. M. Wear-Mode Mapping for the Micro-Scale Abrasion Test. *Wear* **2003**, *255* (1), 23–29.
- (33) Trezona, R. I.; Allsopp, D. N.; Hutchings, I. M. Transitions Between Two-Body and Three-Body Abrasive Wear: Influence of Test Conditions in the Microscale Abrasive Wear Test. *Wear* **1999**, *225 Part 1* (0), 205–214.
- (34) Zou, M.; Yang, D. Nanoindentation of Silica Nanoparticles Attached to a Silicon Substrate. *Tribol. Lett.* **2006**, *22* (2), 189–196.
- (35) Fischer-Cripps, A. C. *Nanoindentation*. Springer: New York, 2011.
- (36) Shorey, A. B.; Kwong, K. M.; Johnson, K. M.; Jacobs, S. D. Nanoindentation Hardness of Particles Used in Magnetorheological Finishing (MRF). *Appl. Opt.* **2000**, *39* (28), 5194–204.